# Space Rapid Transit: Reusable, Two Stage to Orbit, Launch Vehicle with a Hypersonic First Stage

Joyce Mo\*, Michael Paluszek\*

\*Princeton Satellite Systems
6 Market Street, Suite 926 Plainsboro, NJ 08536, USA
map@psatellite.com †Corresponding author · jqmo@psatellite.com ·

### **Abstract**

The expansion of space commercialization demands cost-effective and safe access to orbit. While vertical launches dominate, horizontal launch systems would improve the safety of launch operations and expand accessibility to space by enabling aborts without vehicle destruction and increasing the number of potential launch sites globally. This paper builds on prior work on Space Rapid Transit (SRT), a horizontal, two stage to orbit (TSTO), hypersonic launch vehicle to deliver a 500 kg payload to low earth orbit (LEO). An overview of the design, inlet sizing, concept of operations, trajectory, and estimated research and development costs are presented. Updates include a first stage powered by a hydrogen-fueled ramjet and F135 turbofans and a second stage powered by an RL10 rocket engine. Trajectory optimization achieves stage separation at 39 km and Mach 5.3. This paper also covers the expected development costs based on NASA's Advanced Missions Cost Model.

## 1. Introduction

Two stage to orbit (TSTO) launch vehicles have been conceptualized since the 1960's for on-demand access to low earth orbit (LEO) through horizontal and hypersonic launches. Currently, no TSTO launch vehicles harnessing horizontal take-off are in operation, although TSTO launch vehicles have been proposed or designed at NASA, the China Aerospace Science and Technology Corporation, and Messerschmitt-Bolkow-Blohm (MBB) in the past.<sup>1,2</sup> Of these TSTO vehicles, MBB's Sanger II had been designed in thorough detail for a 10<sup>4</sup> kg payload or 230 passengers if used as a hypersonic airliner. It harnessed a turbo-ramjet powering a hypersonic glider to reach Mach 6.8 and a rocketpropelled second stage to reach LEO. Sanger II's development was halted due to high capital requirements to bring the program to completion.<sup>3</sup> NASA's Beta Launch program was a series of studies between 1986 and 1992 for horizontal takeoff, landing, and launch operations. Gross Lift-Off Weight (GLOW) Space Shuttle replacements studied during that program were for  $2.25 \times 10^4$  kg payload and  $1.125 \times 10^4$  kg payload to LEO. Currently, the majority of launches to LEO are limited to vertical launches, requiring launch sites to be in remote areas and near the equator. The Pegasus XL was the only operating horizontal launch system in use from 1990 to 2021 as a three-stage to orbit, all-solid fueled launch vehicle. The Pegasus XL was lifted to its launch altitude of  $1.2 \times 10^4$  m using the Stargazer L-1011. Then it would free-fall in a horizontal position before igniting the rocket motor.<sup>5</sup> Spaceplanes in operation, including the X-37B and Chinese Reusable Experimental Spacecraft (CSSHQ), still require an initial vertical launch before cruise and numerous stages to orbit. Another spaceplane that was developed was the HOTOL, British Aerospace's reusable, single-stage-to-orbit (SSO) launch concept for a payload of 7 tons to LEO. The HOTOL served to increase the number of launch sites possible and make reusable launches feasible, although it was also terminated due to high program costs.

However, the global space industry has continued to grow, with nearly 200 successful launches to Earth orbit or beyond in 2023 compared to approximately 100 launches in 1991.<sup>6</sup> As the LEO commercial industry expands, improving the accessibility of launches, in terms of cost, frequency, and location, it will be crucial to enable more payloads to be launched on demand. Reusable launch vehicles such as the Falcon 9 have been developed to decrease the cost per kilogram of a payload by saving materials and time between launches. While Falcon 9 has presented cost savings, it still relies on standard vertical launch facilities, limiting the number of potential locations across the globe to launch from. A reusable vehicle with horizontal takeoff presents further advantages in terms of accessibility. Since the Pegasus XL, no horizontal launch vehicles have been fully demonstrated to deliver payloads to orbit. The capability of horizontal launch for space is the concept of a "mobile launch pad" that can use existing aircraft runways, cruise above unwanted weather conditions, loiter for mission instructions, and achieve precise placement for orbital intercept,

#### SPACE RAPID TRANSIT

rendezvous, or reconnaissance. SSO is operationally the simplest for launch, but requires the air-breathing engines to reach orbit, reducing overall payload capacity. TSTO has more complicated ground operations compared to SSO, requiring the mating of two stages. Large TSTO vehicles such as the Sanger II would need dedicated mating facilities. Compared to SSO, the two stages of TSTO launch present flexibility in terms of number of potential applications, whereby each component could be used separately. For instance, the first stage hypersonic aircraft could be used terrestrially as a hypersonic glider for transportation or defense applications.

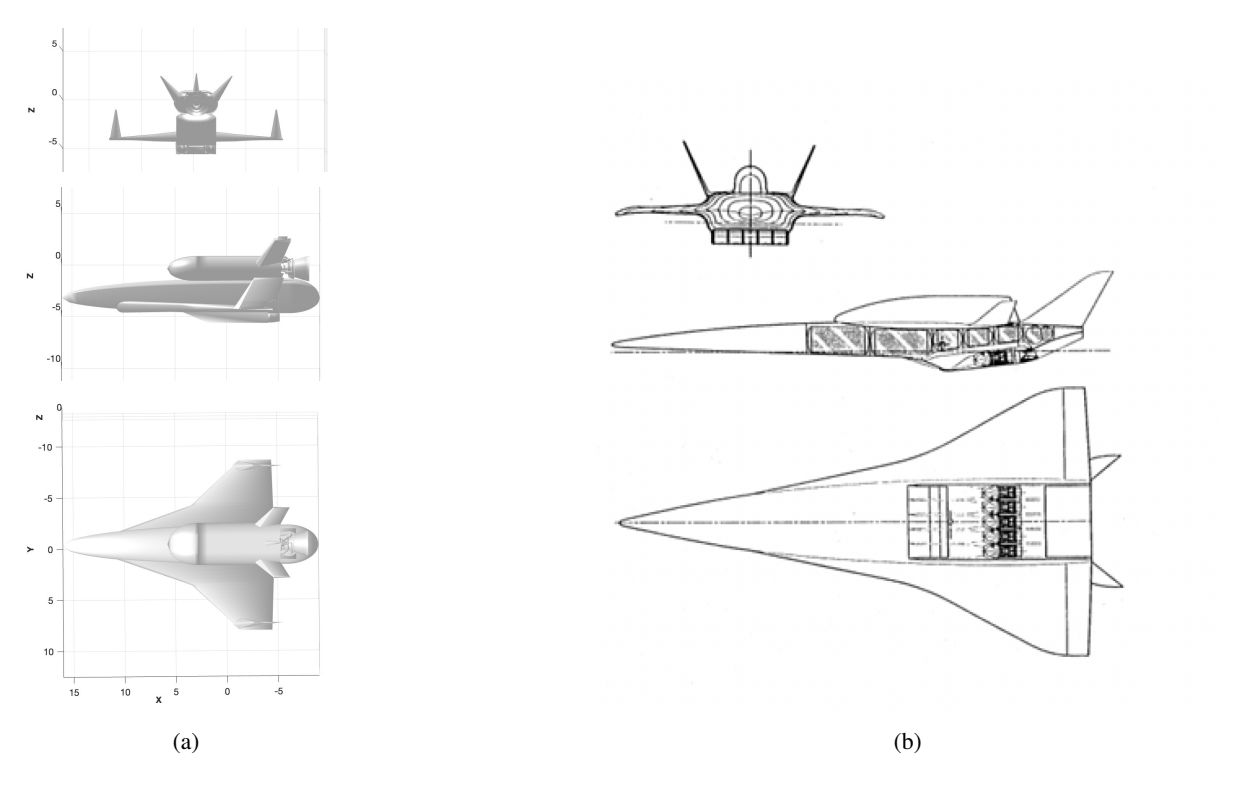


Figure 1: (a) CAD model (units in meters) of SRT designed with the Princeton Satellite Systems Spacecraft Design Toolbox. The length of the Ferry spans 30 m with a 25 m wingspan. The Orbiter is designed to fit the fuselage of the Ferry. (b) Sanger II graphic. The proposed Sanger II length is 84.50 m with a wingspan of 41.40 m.<sup>7</sup>

To meet the demands of the growing space industry, Space Rapid Transit (SRT) is an autonomous TSTO launch vehicle using a hypersonic, air-breathing first stage and rocket-engine-based second stage for a 500 kg payload to LEO. It is currently at technology readiness level (TRL) 2, at a conceptual level of design. Various iterations of SRT have been described in numerous papers, with differences in trajectory and designs based on use of a rotating detonation engine, coaxial turbo-ramjet, or varied payload capacities to LEO.<sup>8–13</sup> This paper covers updates in the propulsion system, airframe, control, material selection, and development costs. In the proposed design, the first stage Ferry harnesses two military-grade jet-fueled F135 turbofans and a hydrogen-fueled ramjet for a horizontal launch. The second stage Orbiter separates from the Ferry using the RL10 fueled by LH<sub>2</sub>/LO<sub>2</sub> to reach LEO. SRT is designed with the biotechnology and pharmaceutical research currently conducted at the International Space Station in consideration. The 500 kg payload is suitable for Starlink units (260 kg),<sup>14</sup> cubesats (0.2 kg to 40 kg), minisatellites (100 kg to 500 kg),<sup>15</sup> or the equipment for biomanufacturing, such as CubeLabs (1.0 kg to 9.0 kg).<sup>16</sup>

# 2. Space Rapid Transit Design

This section discusses the design of the Space Rapid Transit Vehicle. Individually, several components of SRT, such as the RL10, are at TRL 9. Table 1 shows key design features. The airframe sizes are shown in figure 1. The Ferry and Orbiter were sized based on expected fuel requirements based on the trajectory in figure 8. The features selected for SRT serve to lower development timelines by using existing systems, reduce dry mass, and enable quicker turnaround between the construction of new SRT vehicles. For instance, the Moog tubular linear actuators reduce the need for heavy gearboxes and hydraulics that standard electromagnetic actuators require. The reaction control system is a blowdown pressurization system, and the 1N HPGP engines use a non-toxic, green propellant, based on ammonium dinitramide, to simplify ground operations.

Subsystem	Element	Flight Heritage	TRL
Propulsion	Aerojet Rocketdyne RL10	Close derivative of engines used on	9
		GE Series 5000, Mars Observer	
	Pratt&Whitney F135 Turbofan	Lockheed Martin F-35 Fighter	9
	H <sub>2</sub> Ramjet	NASA ground-level tested	3
	Aerojet Rocketdyne fuel tanks	Indostar <sup>19</sup>	9
GN&C	RAD510 processor	InSight Mars Lander and the Mars	9
		Perseverance Rover	
	Air-Data-Sensor-System	Acquisition of data at hypersonic	9
		flight	
	Honeywell HG4934SRS MEMS IMU	Space grade IMU	9
Reaction Control System	Monopropellant HPGP Thrusters	Swedish Space Corporation Prisma	7
Thermal	Radiators (Orbiter)	Deployable with fluid loops	9
	Heat distribution (Orbiter)	Combination of passive and active	9
	RP46 Unidirectional IM7 carbon composites	Unitech	9
Actuation	Moog tubular linear motors	Aerodynamic surfaces, engine gim-	9
		bals, payload doors, landing gear	
		and doors, separation system	

Table 1: Key design elements show extensive flight heritage.<sup>8</sup>

The airframe will be manufactured from carbon composites incorporating a resin polyamide system for the external skin and internal skeleton. Fiber-reinforced composites, such as the RP46 Unidirectional IM7 carbon composite, have higher thermal load capabilities (>1700 ° C) and improved strength-to-weight ratios due to reinforced strength from carbon and ceramic fibers. Refractory ceramics likewise have higher-temperature capabilities (>1700 ° C) but lack thermal shock resistance and tend to be used for thermal barrier coatings. The inlet of the Ferry, in particular, requires higher temperature materials. C/C composites can be used to operate at temperatures for velocities near Mach 6.21

# 2.1 Propulsion System

The first stage Ferry uses a dual-flow path configuration of two jet-fueled turbofans and a LH<sub>2</sub> fueled subsonic ramjet in parallel as shown in figure 2. This is similar to NASA's Beta II concept, which also harnessed jet-fueled turbojets and a LH<sub>2</sub> ramjet. The Ferry's engines would be mounted to the fuselage at the undercarriage aft frame. The ramjet engine follows a similar thermodynamic cycle as the Brayton cycle, whereby the ramjet implements subsonic compression of incoming air, just as the Brayton cycle involves compression of a working fluid. The engine itself does not require mechanical compression. It just uses the momentum of the approaching airflow for the compression required for combustion. Any ramjet engine is comprised of an inlet, combustion zone, and a nozzle.<sup>22</sup> For the operation of SRT, the ramjet is only used as an accelerator to reach Mach 5 after the turbofans reach Mach 1.5. Beyond Mach 6, the subsonic combustion ramjet is less efficient, as the pressure become too high for Brayton cycle operations, and a higher degree of dissociation of the combustion exhaust flow occurs and reduces the overall energy available for the exhaust velocity.<sup>22</sup> The Orbiter uses an LH<sub>2</sub>/LO<sub>2</sub> RL10 from Aerojet Rocketdyne, a flight-tested solid rocket booster used on the Delta IV, Atlas V, Vulcan, and SLS.<sup>23</sup>

The fuel selection is based on specific impulse advantages: liquid hydrogen fuel with liquid oxygen oxidizer enables a specific impulse of 451 s with a 5-1 fuel to oxidizer ratio, compared to the 299 s with liquid methane, 289 s with kerosene, and 303 s with hydrazine, for instance.<sup>23,25</sup> This is in part because hydrogen carries 2.8 times more energy than kerosene for the same mass.<sup>26</sup> The higher the specific impulse, the lower the mass ratio of the vehicle to payload. In addition to the benefit of hydrogen fuel for the specific impulse, hydrogen has lower carbon emissions compared with standard hydrocarbon-based fuels.<sup>27</sup> Hydrogen-fueled ramjets have been developed and tested in wind tunnels by NASA in the 1950s, although the program terminated due to technical challenges with liquefied hydrogen storage.<sup>27</sup> Solid-fueled rocket ramjets have been flight tested, as seen through a successful demonstration of a rocket boosted ramjet sustaining Mach 3 for 3.4 minutes.<sup>28</sup> Hydrogen-fueled turbofans would also have specific impulse improvements, as suggested by the overall comparison of specific impulse of varied engine types in figure 2, but the challenge of sustained hydrogen storage for cruise would need to be considered. Separately, the F135 turbofans and RL10 have reached TRL 9 for jet propellant, in the case of the F135, and LH<sub>2</sub>/LO<sub>2</sub> for the RL10. To simplify the overall SRT design and analysis, the F135 existing engine data sheet for conventional fuel is assumed.

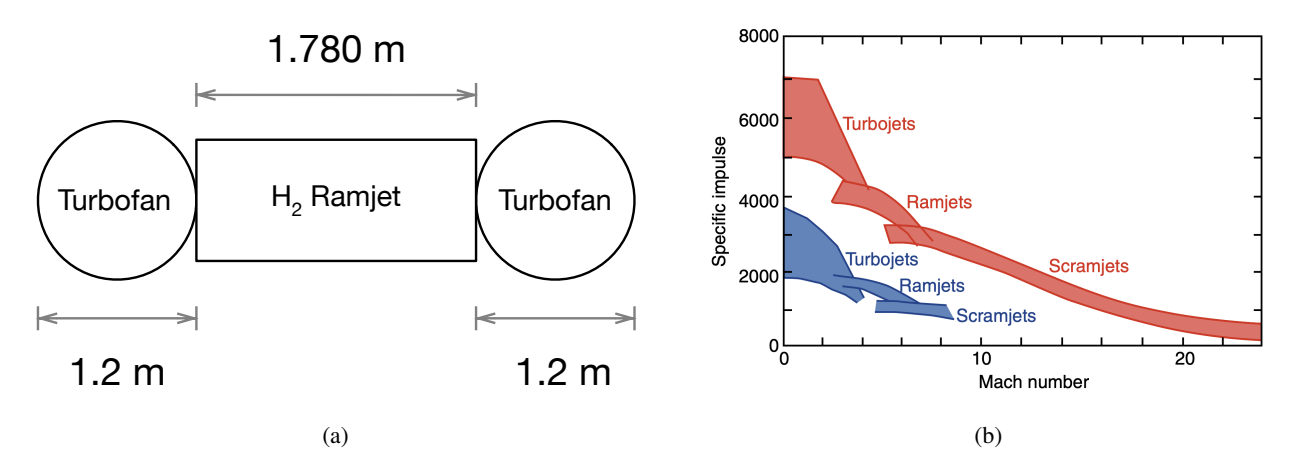


Figure 2: (a) Engine sizing of turbofans and ramjet. (b) Air-breathing engines specific impulse at varied Mach number with hydrogen fuel (red) and conventional hydrocarbon fuel (blue).<sup>24</sup>

Alternatively, an air-breathing rotating detonation engine, detonation ramjet, or coaxial turboramjet could be used for acceleration to the separation altitude, as discussed in prior iterations of SRT.<sup>8</sup> A continuous subsonic ramjet and turbofans were selected to increase the overall average TRL of the total components, whereas developing a coaxial turboramjet requires entirely new engines. Rotating detonation engines face challenges with the stability of detonations tied to the exhaust throat and inlet restriction.<sup>29</sup>

## 2.2 Liquid Hydrogen Storage

Challenges with liquefied hydrogen storage derive from its low boiling point (-252.85°C), requiring cryogenic cooling or passive multi-layer insulation to reduce boil-off. To compensate for the low boiling point, different tank geometry is considered: spherical LH<sub>2</sub> tanks are used in space applications because they require less surface area for a given volume, resulting in less passive heat flux into the tank.<sup>30</sup> The Orbiter would use a spherical tank. Cylindrical tanks, in comparison, have a higher surface area to volume ratio, resulting in higher passive heat flux. Cylindrical tanks with semi-spherical end caps on both ends are used on the Ferry to improve the surface area-to-volume ratio within the fuselage. External insulation, such as that used in the *Cryoplane* project, serves to reduce heat flux further.<sup>26</sup> Jet propellant is also selected for the turbofans in order to reduce the quantity of liquid hydrogen required, which would otherwise need sustained hydrogen storage from takeoff to landing. The volume of the tanks sized for SRT is based on the fuel requirements for atmospheric flight.



Figure 3: Cylindrical tank with spherical end caps sized for Ferry based on fuel mass requirements. Image generated with the Princeton Satellite Systems Spacecraft Design Toolbox. The volume is a factor of 1.2 times larger than required in the event of leakage or evaporation. Axes are in units of meters.

## 2.3 Inlet Design

For an airbreathing propulsion system, the inlet is the component where air flows for entry into the engine. At high speeds, the air must be decelerated to meet the conditions required at the engine face. For this analysis, two main

boundary conditions are considered. The upstream boundary condition is the state of the airflow approaching the inlet, and the downstream boundary condition is the desired state of the airflow for the engine operation. The inlet needs to capture airflow and successfully compress the air to reach the desired downstream boundary conditions and minimize total pressure loss.<sup>31</sup> In general, for each 1% loss in total pressure, a 1.5% loss in engine thrust can be assumed.<sup>32</sup>

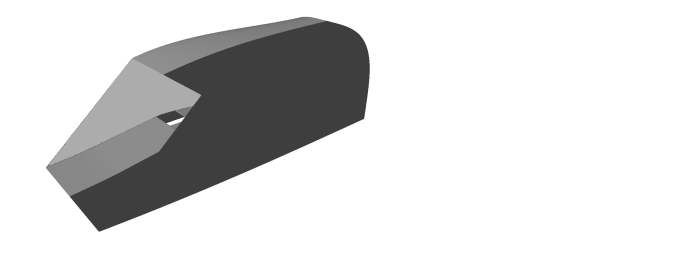
To size the inlets, the Ferry's inlets were designed using the Supersonic Inlet Design and Analysis Tool (SUPIN), a Fortran 95 program that performs geometric modeling, aerodynamic design, and analysis of inlets for a range of Mach numbers. This includes measurements of flow rates, pressure recovery, and drag averaged along a cross-section of the inlet across different regions. In our case, we designed the inlets for the maximum expected freestream Mach number that each engine will operate under. For the turbofans, the freestream Mach number of the upstream boundary condition was set at Mach 1.6, and Mach 5 for the ramjet. This is in line with the highest reported Mach numbers flown using the F135 turbofan. A Mach 6 inlet for the ramjet was initially considered, but trajectory analysis indicates that the ramjet would only reach Mach 5.3 during flight. The analysis by SUPIN assumes adiabatic flow throughout the inlet flowpath, quasi one-dimensional flow, and ideal gas. An iterative procedure was used to size the capture area of the inlet  $A_{cap}$  to establish flow continuity within the inlet and match the downstream boundary conditions specified. The fundamental equations for the flow rate W can be estimated as

$$W = A \frac{P}{\sqrt{T}} \phi \tag{1}$$

where A is the cross-sectional area, P and T are the averaged pressure and temperature at the cross section, and  $\phi$  is the flow function:

$$\phi = M \sqrt{\frac{\gamma}{R} \left( 1 + \frac{\gamma - 1}{2} M^2 \right)^{-\frac{\gamma + 1}{2(\gamma - 1)}}}$$
 (2)

 $\gamma$  is the ratio of specific heats, R is the universal gas constant, and M is the Mach number. From these relations, and estimated mass flow balance throughout the inlet,  $A_{cap}$  can be iterated upon, and flow properties such as pressure and temperature can be numerically estimated.



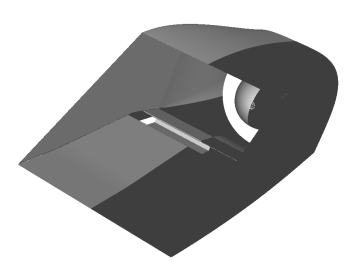


Figure 4: Two views of turbofan inlet with bleed model incorporated.

### 2.3.1 Turbofan Inlet

The inlet is modeled as an external-compression, two-dimensional single-duct inlet for Mach 1.6. The freestream conditions were calculated using standard atmosphere models associated with an altitude of 40 km. The engine-face diameter was 1.2 m with an engine-face Mach number of  $M_{EF} = 0.58$ . The cowl lip angle was specified to be 6 degrees. A shoulder bleed slot was included to remove a small amount of the core inlet flow to improve the boundary layer to better withstand adverse pressure gradients within the inlet flow as the turbofan is within transonic conditions. The F135 engine inlet would also have ramps to open or close depending on whether the Ferry is operating with the turbofans or ramjet.

The reported conditions at station EX represent the state of the flow at the end of the external supersonic diffuser on the upstream side of the terminal shock wave. Station NS represents conditions downstream of the terminal shock wave system modeled as a normal shock wave in SUPIN. The overall pressure recovery with the proposed turbofan inlet is 97.59 %. The inlet would contribute a drag of 5.098 lbf and is 3.05 m in length.

Iteration	p <sub>EF</sub> / p <sub>FS</sub>	M <sub>EF</sub>	$A_{cap}$ (ft <sup>2</sup> )
1	0.963057	0.400000	9.565986
2	0.976474	0.400000	9.620943
3	0.975916	0.400000	9.754981
4	0.975915	0.400000	9.749411

Table 2: Iterations for turbofan inlet sizing, where EF represents the engine face and FS represents freestream.  $p_{EF}$  /  $p_{FS}$  represents pressure recovery ratio of the pressure at the engine face over the freestream pressure.  $A_{cap}$  represents the inlet capture area.  $M_{EF}$  refers to engine face Mach number.

Station	M	$\frac{p_T}{p_{FS}}$	p/p <sub>FS</sub>	T/T <sub>FS</sub>
FS	1.60000	1.00000	1.00000	1.00000
EX	1.30000	0.99847	1.53168	1.13004
NS	0.78596	0.97787	2.76468	1.34574
Cowl lip	0.78596	0.97787	2.76468	1.34574
Throat	0.78596	0.97787	2.76468	1.34574
Subsonic diffuser	0.67490	0.97787	3.06331	1.38576
Engine Face	0.40000	0.97592	3.71505	1.46512

Table 3: Flow properties across varied stations of the turbofan inlets relative to station FS, freestream conditions immediately upstream of the inlet. M stands for Mach number.  $\frac{p_T}{p_{FS}}$  is the ratio of the total pressure over freestream pressure.  $p/p_{FS}$  refers to the pressure recovery ratio of the pressure at that station over the freestream.  $T/T_{FS}$  is the temperature over freestream temperature ratio.

## 2.3.2 Ramjet External Compression Inlet

The ramjet inlet contains an external supersonic diffuser with 3 stages and an isentropic second stage. The altitude for the upstream boundary condition was specified as 40 km. The engine face was a 0.890 m by 1.780 m rectangle. The inlet includes a diffusing isolator, similar to the Mach 4.0 two-dimensional inlet discussed in Slater's work.<sup>31</sup> The engine-face Mach number was specified to be 0.38 according to the frequently used rule of thumb:<sup>34</sup>

$$\frac{M_{EF}}{M_{FS}} = \sqrt{\frac{T_{FS}}{T_{EF}}} \approx \sqrt{\frac{400}{2800}} \approx 0.38$$
 (3)

The length of the external supersonic diffuser was initially input as 2.4 m, and was iterated upon as seen in table 4. The Mach number distribution at the cowl lip was input as 3.8. The ramps were set with a 3 degree inclination. These two inputs were optimized to minimize pressure loss when keeping other constants the same, particularly the upstream boundary condition of Mach 6 at 40 km and downstream boundary condition of Mach 0.38. The Mach number distribution at the cowl lip in particular played a large role in the pressure recovery ratio and the inlet size.

Mach number distribution = 3.8			Mach number distribution = 2.0.				
Iteration	$p_{EF}/p_{FS}$	$M_{EF}$	$A_{cap}$ (ft <sup>2</sup> )	Iterati	on $p_{EF}/p_{FS}$	$M_{EF}$	$A_{cap}$ (ft <sup>2</sup> )
1	0.028220	0.400000	130.922134	1	0.650484	0.287473	130.922134
2	0.159679	0.061800	7.240617	2	0.698200	0.349449	166.901901
3	0.161441	0.375032	40.970585	3	0.696847	0.380888	179.144943
4	0.161461	0.379945	41.422668	4	0.696837	0.380006	178.797760
5	0.161461	0.380000	41.427738	5	0.696838	0.380000	178.795319

Table 4: Comparison of inlet sizing iteration results for two different Mach distributions at the cowl.

With a Mach number distribution set to 3.8 at the cowl, the length of the overall inlet is 13.3 m. With the lower Mach number distribution of 2.0, the overall inlet is 44 m, although it has a superior pressure recovery ratio of 69.68% compared to 16.14%. To reduce mass and drag contributed by the inlet, smaller inlets are favored, although the pressure recovery is lower. The analysis indicates that the inlet is still able to achieve airflow deceleration from Mach 5 to Mach 0.38 even with the smaller inlet. An even smaller inlet in length could converge when optimizing the size on SUPIN; however, this comes at the cost of an even lower pressure recovery ratio.

Station	M	$rac{m{p}_T}{m{p}_{ ext{EF}}}$	$p/p_{\rm EF}$	T/T <sub>EF</sub>
FS	5.00000	1.00000	1.00000	1.00000
EX	3.80000	0.99517	4.54343	1.54321
NS	0.44073	0.16368	75.78430	5.77562
Cowl lip	0.44073	0.16368	75.78430	5.77562
Throat	0.44110	0.16357	75.71867	5.77526
Subsonic diffuser	0.44255	0.16315	75.46152	5.77384
Engine Face	0.38000	0.16146	77.32509	5.83158

Table 5: Ramjet inlet performance summary for a Mach number distribution of 3.8 at the start of the cowl. M stands for Mach number.  $\frac{p_T}{p_{\rm FS}}$  is the ratio of the total pressure over freestream pressure.  $p/p_{\rm FS}$  refers to the pressure recovery ratio of the pressure at that station over the freestream.  $T/T_{\rm FS}$  is the temperature over freestream temperature ratio.

The overall pressure recovery is 16.14% with a drag of 321.69 lbf. The total inlet is 13.3 m in length. With the longer inlet, the forebody of the Ferry could be integrated with the inlet to provide the desired compression. Similarly, the intake for the HOTOL was a Mach 5 expanding 20 ft centerbody. The HOTOL's proposed intakes also harnessed vertical wedges. The vertical wedges provide a pressure recovery of 30%, but resulted in a mass of  $5.3\times10^3$  kg when designed for the Mach 5 operating conditions. The target intake mass for the HOTOL was  $1.31\times10^3$  kg. To reduce the intake mass, the intake was sized for Mach 4 allowing for a  $1.5\times10^3$  kg reduction at the cost of the pressure recovery. Further optimization of the ramp angles could potentially improve the current pressure recovery ratios, although the Mach number distribution in this case played a larger role for each  $\Delta M$ .

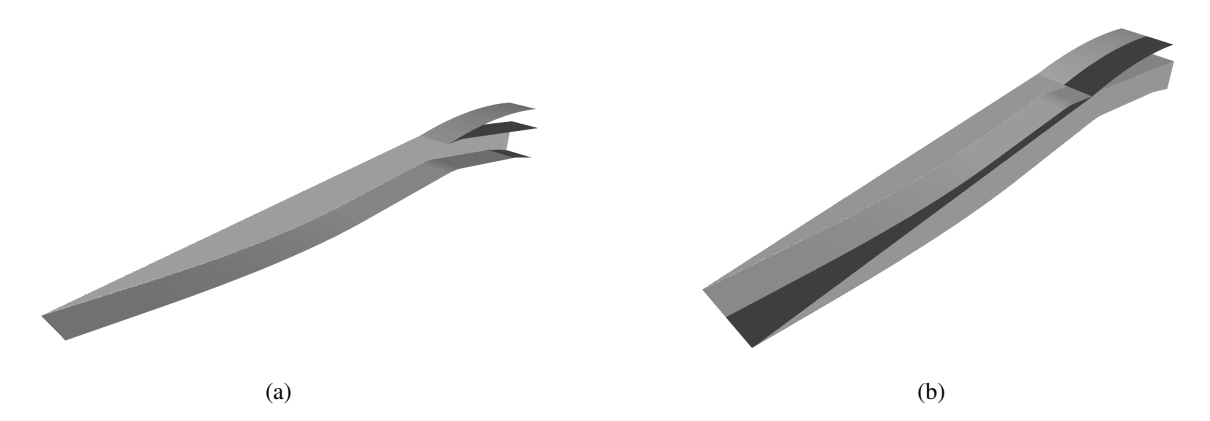


Figure 5: (a) View of a cross-section of the proposed ramjet inlet. (b) Full ramjet inlet.

## 3. Concept of Operations

Since SRT is launched from any airfield with the required 2.27 km airway, specialized launch facilities are not required, opening the possibility of launch from a majority of airports across the globe. In contrast, while not in operation, both stages are housed in standard aircraft hangars and rolled out using standard airport trucks when SRT needs to be used. A Terex AC 40 City Crane, or a similar crane, lifts the Orbiter onto the Ferry. Jet propellant would be loaded first, followed by the RCS HPGP, liquid oxygen, and finally, liquid hydrogen to reduce the risk of evaporation. The liquid hydrogen and liquid oxygen are produced by Air Products. Similar to the Sanger II, the TSTO concept allows for operational flexibility. Due to SRT's cruise capability, it would be able to launch into all orbital inclinations from most airports. It would be able to launch without special launch assist installations, such as sleds and trolleys. In operation, the vehicle trajectory progresses through 7 phases. Aborts do not require the destruction of the vehicle.

- 1. SRT takes off from a runway on turbofans
- 2. SRT accelerates to Mach 1.5.
- 3. Ferry engines switch from turbofans to ramjet for a hypersonic sprint to Mach 5.

### SPACE RAPID TRANSIT

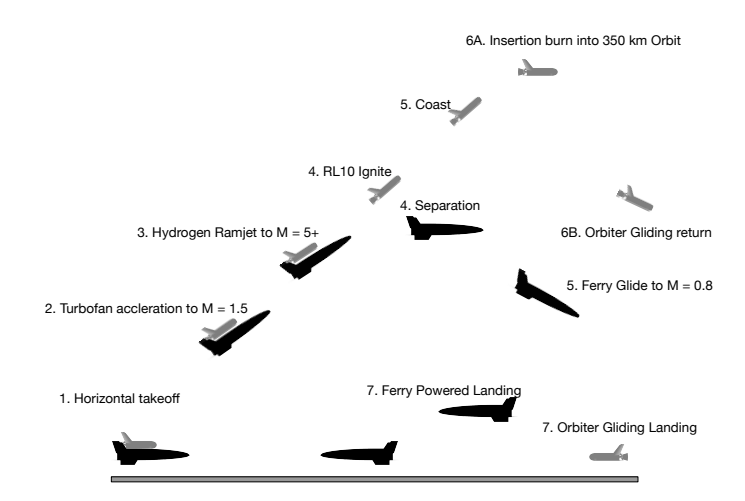


Figure 6: Concept of operations of Space Rapid Transit delivery of a 500 kg payload to LEO.

- 4. Stage separation occurs, and the RL10 ignites for the Orbiter to proceed with a burn to reach the ascending leg of an elliptical transfer orbit. All the while, the Ferry glides to Mach 0.8 on turbofans, and the ramjet is turned off.
- 5. The Orbiter coasts before one final burn to circularize the orbit to 350 km.
- 6. The Orbiter undergoes re-entry.
- 7. The Ferry undergoes a powered landing while the Orbiter follows a glide landing.

# 4. Guidance, Navigation, and Control

The Ferry and Orbiter have independent control systems and are fully autonomous. 10 The control system architecture is presented in figure 7.

A pre-computed optimal trajectory provides reference commands for the velocity  $V_c$  and flight path angle  $\gamma_c$ , which were tweaked by trial and error to obtain an optimal path. The heading command  $\psi_c$  is computed based upon the Earth's rotational velocity and the current airspeed V to provide an inertial azimuth angle equal to  $\beta$ , is:

$$\sin \psi_c = -\epsilon \cos^2 \beta + \cos \beta \sqrt{\tan^2 \beta - \epsilon^2 \sin^2 \beta} \tag{4}$$

where  $\epsilon = \frac{V_E}{V}$  and  $V_E = R_E \omega_E \cos \theta$  is the rotational velocity of the Earth. Let  $V_E \to 0$  for the heading command to become equivalent to the inertial azimuth angle. The desired time derivatives for flight path angle and heading are defined as:

$$\dot{\gamma}_{Des} = K_{\gamma} \left( \gamma_c - \gamma \right) \tag{5}$$

$$\dot{\psi}_{Des} = K_{\psi} \left( \psi_c - \psi \right) \tag{6}$$

where  $K_{\gamma}$  and  $K_{\psi}$  are control gains that may be scheduled to provide the desired performance across the flight envelope. The  $\dot{\gamma}_{Des}$  command is limited by the maximum allowable normal acceleration,  $n_{\max}$ , so that:

$$|\dot{\gamma}_{Des}| \le \frac{n_{\text{max}}}{V} \tag{7}$$

The required commands for the angle of attack and bank angle are determined through the equations of motion for a point mass aircraft. The equations are:

$$\dot{V} = \frac{1}{m} \left( T - \frac{1}{2} \rho(h) V^2 S C_D(\alpha) \right) \tag{8}$$

$$\dot{\gamma} = \frac{1}{m} \left( \frac{1}{2} \rho(h) V S C_L(\alpha) \right) - \frac{g \cos \gamma}{V} \tag{9}$$

$$\dot{h} = V \sin \gamma \tag{10}$$

$$\dot{h} = V \sin \gamma \tag{10}$$

$$\dot{\psi} = \frac{\rho(h)VSC_L(\alpha)\sin\phi}{2m\cos\gamma} \tag{11}$$

S is wetted area,  $C_D$  is the drag coefficient,  $C_L$  is the lift coefficient, g is the acceleration of gravity,  $\alpha$  is angle of attack and h is altitude. The angle of attack can be used to track the flight path angle:

$$\alpha_c = C_L^{-1} \left( \frac{2m \left( \dot{\gamma}_{Des} + g \cos \gamma / V \right)}{\rho(h) V S} \right)$$
 (12)

where  $C_L^{-1}$  represents the inverse function of the lift coefficient. The lift coefficient function is modeled as a function of angle of attack, altitude and Mach number. Using bank angle to track heading, the following relation is obtained:

$$\phi_c = \sin^{-1} \left( \frac{2m \cos \gamma \dot{\psi}_{Des}}{\rho(h) VS C_L(\alpha)} \right)$$
 (13)

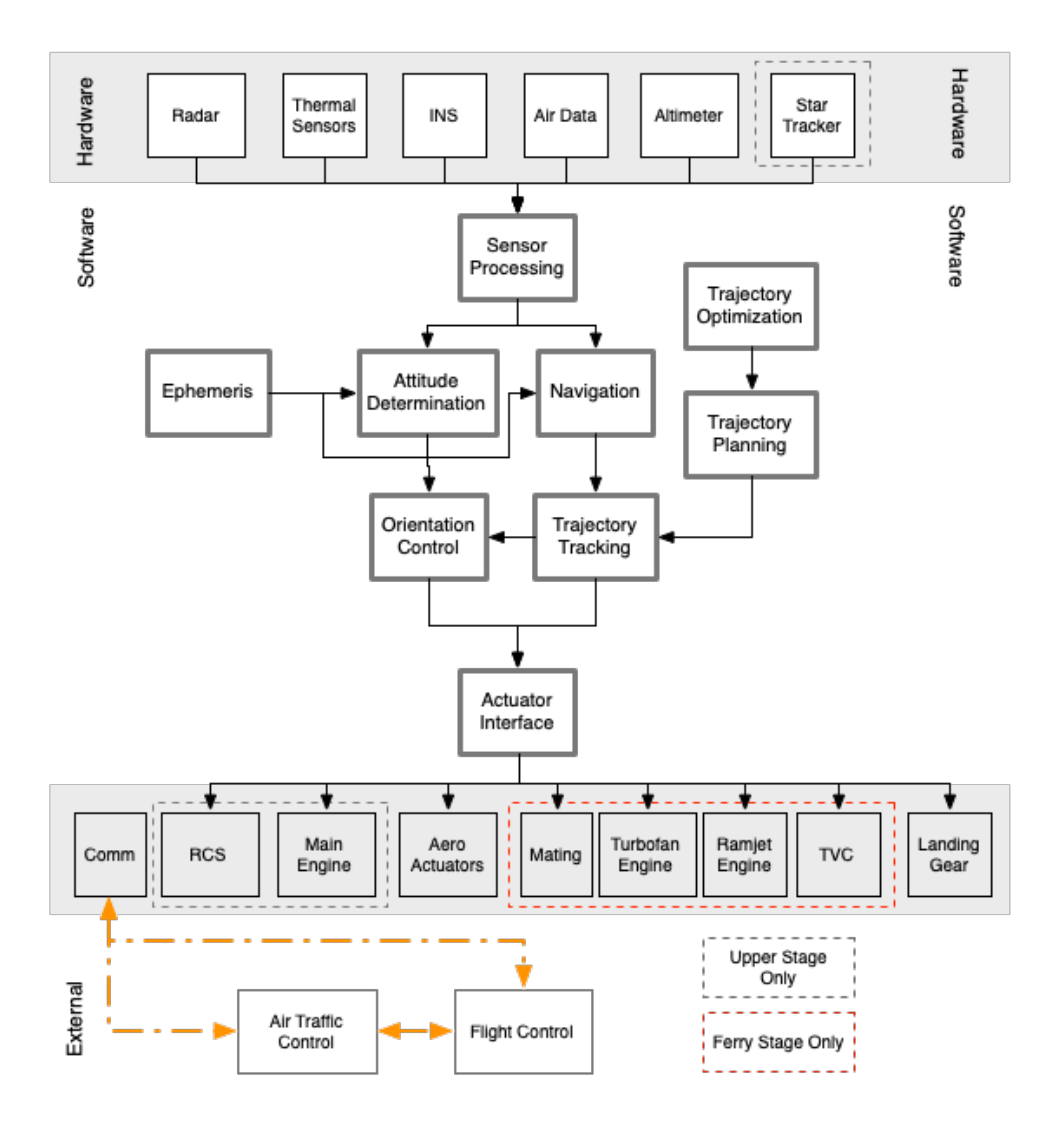


Figure 7: Unified control architecture for SRT.<sup>8</sup>

# 5. Trajectory

The guidance objective during this flight aims for a stage separation at 40 km and a 350 km final altitude for the Orbiter. The constraint placed on the ramjet was for a maximum Mach number of 6.0. The stage separation velocity selected is in line with the stage separation Mach number chosen for the Sanger II, Mach 6.8. The optimization method used for this analysis divides the trajectory of SRT to 350 km altitude into discrete intervals between three major phases, where first the SRT is only propelled by turbofans, followed by the ramjet, and finally the RL10.  $\gamma$  was set as  $\gamma_{turbofan} = 0.2443$  and  $\gamma_{ramjet} = 0.3281$ . The second stage Orbiter, or the third phase of the optimization, follows the relations from Paluszek et al.<sup>13</sup> The boost phase consists of the initial insertion burn that puts the Orbiter into a coast arc. The circularization burn puts it into the drift orbit. The engine has a two-axis gimbal for pitch and yaw control. Roll control is accomplished with the aerodynamic effectors and with the reaction control system. The optimized launch trajectory to 350 km is depicted in figure 8. Within 6 minutes, SRT is able to reach the 350 target altitude and achieve separation at 39.02 km as seen in figure 8. Although the ramjet is defined to reach a maximum Mach number of 6, it does not need to accelerate to those speeds and instead reaches Mach 5.3. The ramjet only needs to operate for 2 seconds for the hypersonic sprint to the separation altitude. This assumes that the Ferry switches from the turbofans at Mach 1.5. The control profile of the Ferry is depicted in figure 8.

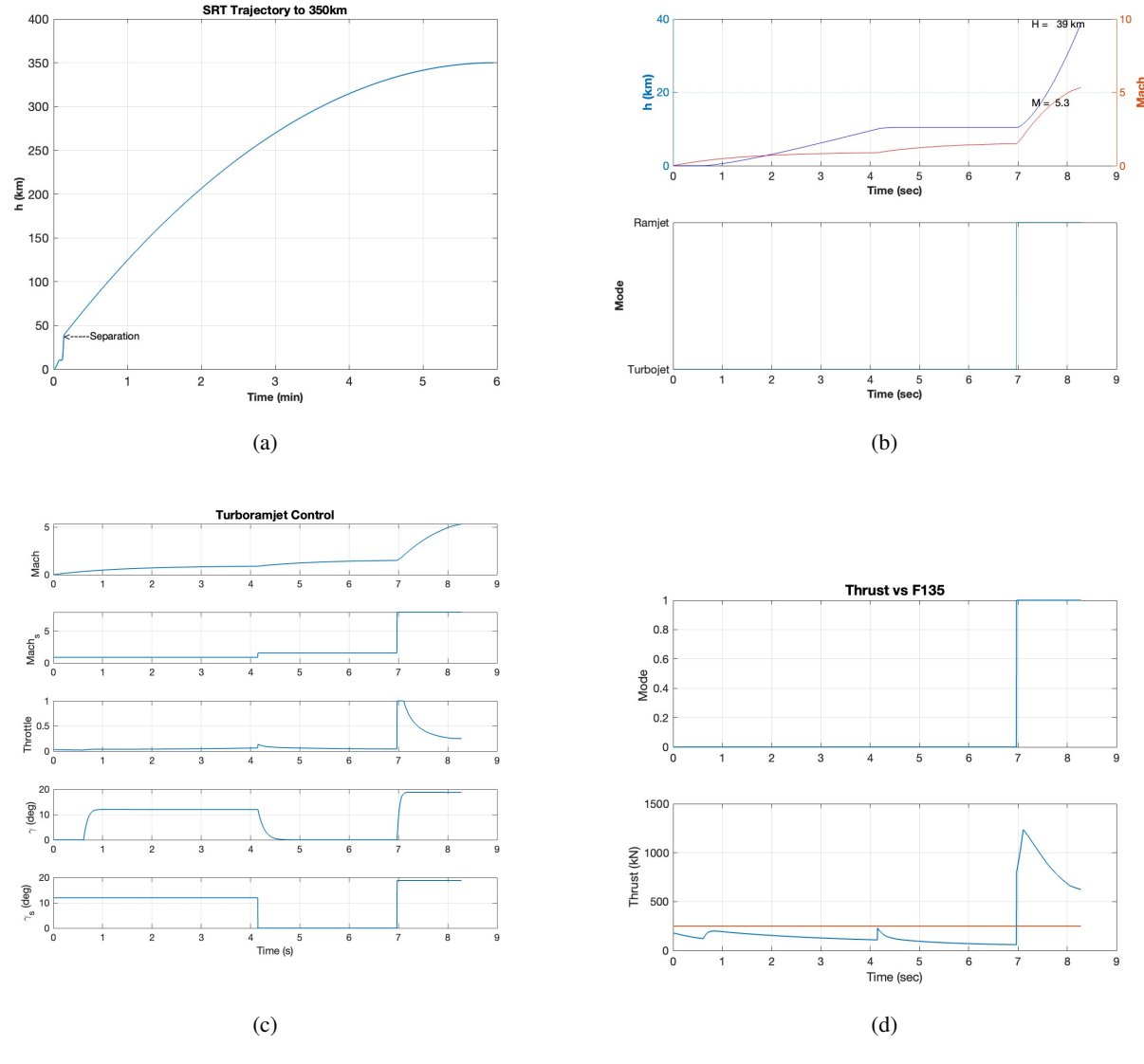


Figure 8: Flight to 350 km. (a) Trajectory of SRT to ISS altitudes (350 km). (b) Ferry height and Mach profile during launch (0 to 10 seconds). (c) Ferry thrust, fuel usage, throttle, and specific impulse. (d) F135 engine thrust profile.

# 5.1 First and Second Stage Profile

The overall parameters based on the trajectory optimization are presented below for the Ferry and Orbiter.

Table 6: First and Second Stage Data

Ferry			
Parameter Value			
Dry Mass	43 785.60	kg	
Fuel Mass	2685.00	kg	
Volume	93.80 r	$n^3$	
Surface Area	631.96	$m^2$	
Takeoff Distance	$2.27  \mathrm{k}$	m	
Mass JP	1234.16	kg	
Mass H <sub>2</sub>	1450.84	kg	

Orbiter				
Parameter	Value			
True Anomaly Separation	3.13 rad			
Separation Velocity	1.69 km	$s^{-1}$		
Flight Path Angle	0.33 rad			
Separation Altitude	39.02 km			
Drag Loss $\Delta V$	0.19 km	$s^{-1}$		
Total $\Delta V$	6.74 km	$s^{-1}$		
Insertion $\Delta V$	3.90 km	$s^{-1}$		
Circularization $\Delta V$ 2.65 km				
Required Mass Fuel	18 256.66	kg		

# 6. Safety and Reliability

Safety is of utmost priority for the design and operations of SRT. The figures of merit NASA and DARPA defined when assessing the safety of horizontal launch concepts are loss of vehicle probability by stage, determined by the number of engines, inherent reliability, stage complexity, emergency stage separation complexity, and number of stage return options. The more engines and stages, the more likely failure will occur. With a total of two stages, 2 engines for the Ferry, and 1 engine for the Orbiter, there are overall fewer stages and engines required with the goal to reduce operational complexity. SRT's operation requires only one staging separation event during its trajectory. The risk from flying at hypersonic speeds comes from the possibility of inlet unstart, where internal shock waves are expelled upstream out of the inlet aperture, causing reduced thrust and drag. Control systems need to be able to handle all conditions of flight. Plasma formation, causing blackout, is not a major concern since SRT does not reach Mach 12, when plasma formation starts to occur. Moreover, the design as a horizontal launch vehicle presents safety advantages over vertical launches. The capability of horizontal launches and landings allows for any stage configuration to glide upon engine failure, rather than destruction of the entire vehicle. For instance, the Ferry is able to operate on the turbofans at subsonic speeds in case of a malfunction of the ramjet. Horizontal launches, as seen through standard commercial passenger airplanes, have a lower fatality rate compared with rockets.

In terms of the reliability of SRT as a reusable launch vehicle, comparisons are drawn with Sanger II as a similar TSTO launch concept. Factors such as mean time between maintenance, stage integration, and propellant storage requirements determine the minimum turnaround time between multiple launches. Surge call-up time, defined as the time between the announcement of a surge mission need and launch, are impacted by the complexity of payload integration, time to refuel tanks, and mission software load time.

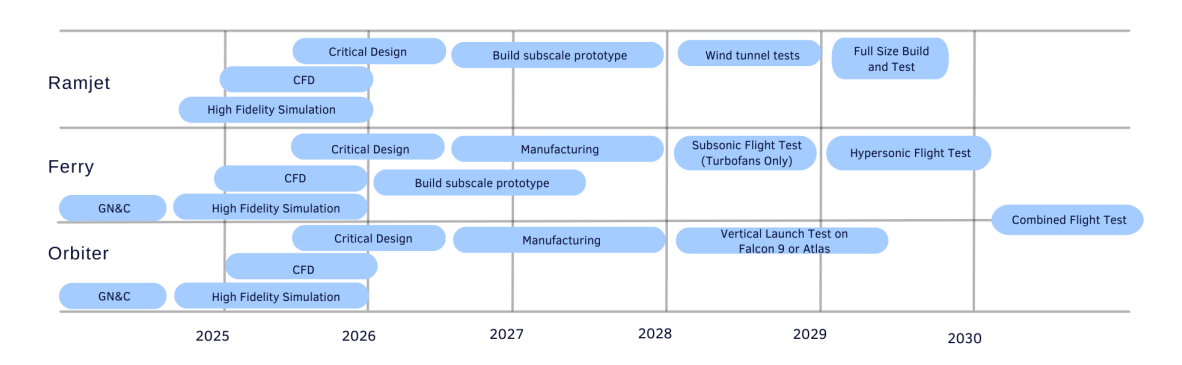


Figure 9: Development timeline for SRT

## 7. Development

The two stages of SRT could be developed in parallel as seen in figure 9. The Orbiter could be flight tested on an Atlas V or Falcon 9 launch if the Ferry is not ready for operation, for instance. This enables the separate components of SRT to reach TRL 9 sooner.

### 8. Business Model

The commercial industry for LEO includes the following sectors: satellite deployment, space tourism, manufacturing and research, space-based energy for the grid, space logistics and transportation, debris management, and commercial space stations. Satellite deployment and services include communication satellites and earth observation for environmental monitoring, agriculture, and disaster response. Along with satellite deployment comes debris management.<sup>37</sup>

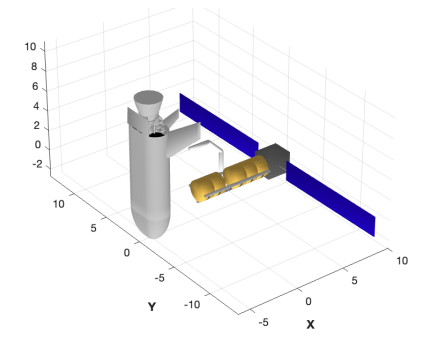


Figure 10: Conceptual space station specific for biomanufacturing with the Orbiter.

Among these sectors of the commercial LEO industry, SRT has the potential to serve several: satellite deployment, manufacturing and research, and largely the space logistics and transportation sector. The intersection between biotechnology and microgravity lies in the manufacturing and research in microgravity. The LEO environment allows for the production of certain materials, pharmaceutical compounds, and drugs that are otherwise difficult to produce on Earth. Companies and research institutions, such as Bristol Myers Squibb and Stanford University, are harnessing microgravity conditions to advance pure biology research, particularly for regenerative medicine, cell analysis, and protein crystallization growth for structural analysis of enzymes.<sup>38</sup> For the biomanufacturing and research sector to expand, more frequent launches are required, however. For instance, if a patient needed a stem-cell derived product, waiting a year for the next launch could be too long for the timescale of an acute cancer condition, which spreads quickly.<sup>39</sup> SRT could become profitable with frequent, on-demand launches with a higher price per kilogram, or as a launch vehicle sold to each country or group interested in obtaining their own launch vehicle to launch from an airport. Lower launch costs of \$300 USD per kg would be feasible if a quantity of 400 SRT vehicles were produced and sold, roughly 2 units per country.<sup>8</sup> Lower launch costs would enable more frequent launches and lower the barrier to entry for commercial activity.

In general, reusable systems have large development costs, requiring many flights to amortize the initial investment. The RDT&E cost of one SRT launch vehicle is \$8.7 billion USD, according to a 2014 estimation of an SRT launch program for a 600 kg payload to LEO using the Roskam airplane cost model. The expected development costs for the updated SRT designs are expected to be lower due to the lower total system mass designed for the overall smaller payload. NASA's Advanced Missions Cost Model (AMCM) estimates a development cost ranging between \$7.6 billion USD to \$13.4 billion USD when accounting for inflation between 1999 to 2024. The AMCM is a long-range forecasting tool to allow quick estimates of program costs during the early conceptual stage. The selection of existing systems, such as the F135 turbofans and RL10, is chosen to lower development costs and quicken development timelines. Thus, the actual cost of the full SRT program may be on the lower end of the projected range. Between launches, SRT may have similar refurbishment costs as the X-15, a hypersonic glider developed in the 1960s. The X-15's refurbishment costs totaled 0.3% of the total program cost, or around \$300 000 between flights. The selection of the projected range for the total program cost, or around \$300 000 between flights.

# 9. Conclusions

Updated designs of SRT are presented, including inlet optimization, airframe sizes, trajectory analysis, and development plans. SRT could act as an impetus for economic growth, particularly for nations that otherwise rely on launch

sites located elsewhere to launch from local airports with a 2.27 km airway. SRT would be able to expand space access to nearly every country, allowing for more people to partake in the global space industry. SRT provides a path to advanced space transportation and advanced commercial LEO operations, fitting within timelines required of typical manufacturing in the biotechnology industry.

Analyses were completed using the Princeton Satellite Systems MATLAB Spacecraft Design Toolbox and SUPIN. To better understand the formation of plasma during re-entry, ongoing work on plasma in hypersonic modeling will aid analysis of the full takeoff to re-entry of the Orbiter and provide insight into how to mitigate effects from drag reduction or communication blackout.

Future work includes higher-order computational fluid dynamics analysis of material selection, insulation thickness, and weight of components such as the hydrogen storage tanks and airframe. The inlets could also be refined further. Within the modeled boundary layers on SUPIN, further boundary layers and shock interactions within were not modeled yet. Computational fluid dynamics studies would be able to provide temperature, Mach number, and pressure distribution of each discretized cell within the inlet, rather than just of the averaged cross-sectional area of the presented regions. The parameters estimated between SUPIN and Wind-US, a CFD software, suggest that the general parameters analyzed on SUPIN are not drastically different from CFD results, as seen in other papers directly comparing the pressure recovery, Mach, and temperature. 31,43

# 10. Acknowledgments

We would like to thank John Slater for his advice on designing inlets for hypersonic engines. We would also like to thank Emma Smithwick for her contributions to a conceptual space station, Dr. Christopher Galea for his input on SRT, and Sarah Fry, who examined the trajectory optimization objective as well.

# 11. Acronyms

Acronyms are given in Table 7.

Table 7: Acronyms.

Acronym	Description
CAD	Computer Aided Design
SRT	Space Rapid Transit
TRL	Technology Readiness Level
LEO	Low Earth Orbit
TSTO	Two Stage to Orbit
SSO	Single Stage to Orbit

## References

- [1] Paul A. Bartolotta, Elizabeth Buchen, Walter C. Engelund, Lawrence D. Huebner, Paul L Moses, Mark Schaffer, Randall T. Voland, David F. Voracek, and Alan W. Hilhite. Horizontal launch: A versatile concept for assured space access. Technical Report SP 2011-215994, NASA, 2011.
- [2] David Shats and Peter Wood. Chinese spaceplane programs. Technical report, China Aerospace Studies Institute, 2021.
- [3] S. Weingartner. Sänger the reference concept of the german hypersonics technology programme. Number AIAA 93-5161, 1993.
- [4] Leo Burkardt and Rick Norris. The design and evolution of the beta two-stage-to-orbit horizontal takeoff and landing launch system. In AIAA 4th International Aerospace Planes Conference, Orlando FL, 1992.
- [5] M. N. Rhode and W.C. Eugelund. Experimental aerodynamic characteristics of the pegasus air launched-booster and comparisons with predicted and flight results. *AIAA*, NASA-TM-112004, 1995.
- [6] Aeronautics and space report of the president fiscal year 2023. Technical report, NASA, 2023.
- [7] P.W.Sacher. Engineering engine/airframe integration for fully reusable space transportation systems. Technical Report RTO-EN-AVT-185, NATO/OTAN, 2010.
- [8] J. B. Mueller and M. A. Paluszek. Space Rapid Transit A Two Stage to Orbit Fully Reusable Launch Vehicle. In *International Astronautical Congress*, number IAC-14,C4,6.2, October 2014.
- [9] Michael Paluszek, Christopher Galea, Miles Simpkins, Yiguang Ju, and Mikhail Shneider. Rotating Detonation Engine for Hypersonic Flight. In *HiSST 2022*, September 2022.
- [10] J. B. Mueller, P. R. Griesemer, M. A. Paluszek, and J. Du. Unified gn&c system for the space rapid transit launch vehicle. In *AIAA GN&C Conference*, August 2010.
- [11] P.R. Griesemer, J.B. Mueller, M.A. Paluszek, and P. Raghavan. Space rapid transit navigation and control. In *EUCASS 2011*, St. Petersburg Russia, July 2011.
- [12] P.R. Griesemer, J.B. Mueller, M.A. Paluszek, and E. de Castro. Space rapid transit for rapid spacecraft deployment. In 2011 Reinventing Space Conference, Los Angeles, California, July 2011.
- [13] Michael A. Paluszek, Christopher Galea, and Stephanie Thomas. Two stage to orbit using a hypersonic first stage and horizontal launch. HiSST, 2024.
- [14] David R. Williams. Starlink 1010, 2019.
- [15] Erik Kulu. What is a nanosatellite?, 2025.
- [16] Inc. Space Tango. Cubelab interface control document, January 2019.
- [17] Moog. High performance linear servomotor, 2014.
- [18] K. Anflo, S. Persson, P. Thormahlen, G. Bergman, T. Hasanof, T-A. Gronland, and R. Mollerberg. GREEN PROPULSION FOR SPACECRAFT-TOWARDS THE FIRST FLIGHT OF ADN BASED PROPULSION ON PRISMA IN 2009. In *International Astronautical Congress*, number IAC-06-C4.1.08, 2006.
- [19] Marvin Arluk, Derek M. Surka, Michael A. Paluszek, and Wendy I. Sullivan. Indostar-1 early orbit operations. 22nd Annual AAS Guidance and Control Conference, (AAS 99-071), 1971.
- [20] Adam B. Peters, Dajie Zhang, Samuel Chen, Catherine Ott, Corey Oses, Stefano Curtarolo, Ian McCue, Tresa M. Pollock, and Suhas Eswarappa Prameela. Materials design for hypersonics. *Nature Communications*, 15(3328), April 2024.
- [21] Krishnam Suhrutha and G Srinivas. Recent developments of materials used in air breathing and advanced air breathing engines. Materials Science Engineering, 2020.
- [22] J. Mattlingly. Elements of Gas Turbine Propulsion. McGraw-Hill, 2005.

- [23] R110 propulsion system. Data Sheet.
- [24] David M. Van WIe, Stephen M. D'Alessio, and Michael E. White. Hypersonic airbreathing propulsion. *Johns Hopkins APL Technical Digest*, 26(4), 2005.
- [25] K. Burke. 4.02 current perspective on hydrogen and fuel cells. In Ali Sayigh, editor, *Comprehensive Renewable Energy*, pages 29–63. Elsevier, Oxford, 2012.
- [26] Bhupendra Khandelwal, Adam Karakurt, Paulas R. Sekaran, Vishal Sethi, and Riti Singh. Hydrogen powered aircraft: The future of air transport. *Progress in Aerospace Sciences*, 60:45–59, 2013.
- [27] Yasin Şöhret, Selcuk Ekici, and T. Hikmet Karakoc. Using exergy for performance evaluation of a conceptual ramjet engine burning hydrogen fuel. *International Journal of Hydrogen Energy*, 43(23):10842–10847, 2018. The 2nd International Hydrogen Technologies Congress (IHTEC-2017).
- [28] Paul J. Waltrup, Michael E. White, Frederick Zarlingo, and Edward S. Gravlin. History of ramjet and scramjet propulsion development for u.s. navy missiles. Technical Report Volume 18, Number 2, Johns Hopkins APL Technical Digest, 1997.
- [29] Daniel E. Paxson and Douglas A. Schwer. Operational stability limits in rotating detonation engine numerical simulations. volume 0748, 2019.
- [30] Xi wan Sun, Zhen yun Guo, and Wei Huang. Passive zero-boil-off storage of liquid hydrogen for long-time space missions. *International Journal of Hydrogen Energy*, 40(30):9347–9351, 2015.
- [31] John W. Slater. Design and analysis tool for external-compression supersonic inlets. AIAA, 0016, 2012.
- [32] J. Seddon and E.L. Goldsmith. Intake Aerodynamics. AIAA Education Series, New York, NJ, 1985.
- [33] Jeremiah Gertler. F-35 alternate engine program: Background and issues for congress, 2012.
- [34] W.H Heiser and D. T. Pratt. Hypersonic Airbreathing Propulsion. AIAA Education Series, 1999.
- [35] Dan Sharp. HOTOL Britain's Spaceplane. Tempest Books, 2024.
- [36] R.B. Miles and Mikhail Shneider. Magnetohydrodynamic and electrodynamic control of hypersonic flows of weakly ionized plasmas. *AIAA Journal*, 42(7), 2004.
- [37] Commercial market assessment for crew and cargo systems pursuant to section 403 of the nasa authorization act of 2010. Technical report, NASA, 2011.
- [38] Arun Sharma, Rachel A Clemens, Orquidea Garcia, D Lansing Taylor, Nicole L Wagner, Kelly A Shepard, Anjali Gupta, Siobhan Malany, Alan J Grodzinsky, Mary Kearns-Jonker, Devin B Mair, Deok-Ho Kim, Michael S Roberts, Jeanne F Loring, Jianying Hu, Lara E Warren, Sven Eenmaa, Joe Bozada, Eric Paljug, Mark Roth, Donald P Taylor, Gary Rodrigue, Patrick Cantini, Amelia W Smith, Marc A Giulianotti, and William R Wagner. Biomanufacturing in low earth orbit for regenerative medicine. *Stem Cell Reports*, 17(1):1–13, Jan 2022.
- [39] Anjali Prashar, Faraha Siddiqui, and Amit Kumar Singh. Synthetic and green vegetable isothiocyanates target red blood leukemia cancers. *Fitoterapia*, 83(2):255–265, 2012.
- [40] H.S. Becker. Design and economic aspects of reusable launch vehicles and considerations for future systems. *NASA Technical Memorandum*, 1968.
- [41] Harry W. Jones. Estimating the life cycle cost of space systems. NASA, 45th International Conference on Environmental Systems, 2015.
- [42] James E. Love and William R. Young. Survey of operation and cost experience of the x-15 airplane as a reusable space vehicle. *NASA Technical Note*, D-3732, 1966.
- [43] Lee M. Berra, John W. Slater, and Semih M. Olcmen. Conceptual redesign of the b-1b bomber inlets for improved supersonic performance. *Aerospace Science and Technology*, 45:476–483, 2015.